DOI: 10.1002/ ((please add manuscript number))
Article type: ((**Full Paper**))

Manipulation of Disodium Rhodizonate: Factors for Fast-Charge and -Discharge Sodium-Ion Batteries with Long-Term Cyclability

*Chengliang Wang, Yaoguo Fang, Yang Xu, Liying Liang, Min Zhou, Huaping Zhao, and Yong Lei**

Dr. C. Wang, Y. Fang, Dr. Y. Xu, L. Liang, Dr. M. Zhou, Dr. H. Zhao, Prof. Y. Lei
Institute of Physics & IMN MacroNano®
Technical University of Ilmenau, Ilmenau 98693, Germany
E-mail: yong.lei@tu-ilmenau.de

Keywords: organic sodium-ion batteries, cathodes, long-term cyclability, fast-charge, binders

Abstract: Organic sodium-ion batteries (SIBs) are one of the most promising alternatives of current commercial inorganic lithium-ion batteries (LIBs) especially in the foreseeable large-scale flexible and wearable electronics. However, only a few reports are involving organic SIBs so far. The fast-charge and -discharge performance and the long-term cycling, which are extremely important for practical applications, are still challenging. Here, important factors for high performance SIBs especially with high capacity and long-term cyclability under fast-charge and -discharge process are investigated. We found that controlling the solubility through molecular design and determination of the electrochemical window is essential to eliminating the dissolving of the electrode materials and thereby improving the cyclability. The results show that PVDF will decompose during the charge/discharge process, indicating the significance of the binder for achieving high cyclability. Beside of these, we also show that decent charge transport and ionic diffusion are beneficial to the fast-charge and -discharge batteries. For instance, the flake morphology facilitates the ionic diffusion and thereby can lead to a capacitive effect that is favorable to fast-charge and -discharge.

1. Introduction

Due to the abruptly increasing demand of lithium-ion batteries (LIBs) in powering portable electronic devices (especially the burgeoning flexible and wearable electronics) and electric vehicles and the concern of limited Li resources, sodium-ion batteries (SIBs) have attracted more and more attention for the foreseeable large-scale applications because of the similar electrochemical properties (same main group and only 0.3 V more positive), the environmental benignity and the abundance of Na compared with Li.[1-7] The conventional inorganic materials used as cathodes in LIBs and SIBs involving transition metal elements are facing the challenges of limited resources, non-degradability and complex purification and syntheses. However, the organic materials are free from these problems.[8-32] Moreover, the large size of Na ions and the rigid structure of inorganic materials always lead to an irreversible morphological or structural deformation of the electrodes after the intercalation of Na ions (e.g. about 400% volume expansion for Sb[1, 3] and Sn[5] electrode). Such huge volume change would devastate the electrode structures and result in poor cyclability. Different from inorganic materials, organic materials possess soft and flexible structures and our previous work have proved that the volume change of organic electrode materials after intercalation of Na ions could be negligible, especially for the layer-by-layer materials.[12] Beside of these advantages, organic materials can also be functionalized through chemical syntheses, which is promising for adjusting the physical and electrochemical properties. An example is that the groups connected to the carbonyl group which is a functional site for intercalation/extraction of Na ions can change the electrochemical potential (*vs*. Na/Na^+) significantly. Generally speaking, the carbonyl group in the carboxylate[10-16] leads to a potential (e.g. <1 V) close to that of Na/Na^+, which is suitable for anode materials in the SIBs. While the keto-carbonyl[10, 16-19, 21-23, 30, 31] gives a potential around 2~3 V (*vs*. Na/Na^+), which can be used as potential cathodes in SIBs. However, till now, only a few reports are focusing on organic sodium-ion batteries[12-17, 22-27] and organic materials for cathodes[16, 17, 22-25] are

particularly challenging. Moreover, for portable electronics, a battery without significant fade after more than 1100 cycles (three years, if charged once per day) is a basic requirement, which, however, is rarely reported. Additionally, the fast-charge and -discharge performance, which are also very important for practical applications, are either not reported or suffered dramatic decay.

Herein, important factors for fast-charge and -discharge organic sodium-ion batteries with high capability and long-term cyclability will be investigated by using rhodizonate (its lithium salt is widely studied in LIBs)[18, 19, 33, 34] which contains pairs of keto-carbonyl groups as a model. We found that controlling the solubility through molecular design and determination of the electrochemical window is essential to eliminating the dissolving of the electrode materials and thereby improving the cyclability. The results showed that PVDF, which is stable and widely adopted in LIBs and SIB, however, will decompose during the charge/discharge process, indicating the significance of the binder for achieving high cyclability. Beside of these, we also showed that decent charge transport and ionic diffusion are beneficial to the fast-charge and -discharge batteries. For instance, the flake morphology facilitates the ionic diffusion and thereby can lead to a capacitive effect that is favorable to fast-charge and -discharge.

2. Results and discussion

2.1 Molecular design

In order to design a cathode material by using keto-carbonyl groups with high specific capacity, one possible design strategy is to propose a material in which every carbon exists in the form of keto-carbonyl. In this case, the molecular formula can be written as $(CO)_n$. Every keto-carbonyl group could accept one electron and one sodium cation, forming $(CO)_n^{n-}Na_n^{n+}$, leading to a theoretical specific capacity of 957 mAh g^{-1}, which is quite encouraging for cathodes in organic sodium-ion batteries. Importantly, our previous work[12] has shown that the electron withdrawing group can increase the electrochemical potential (*vs*. Na/Na^+) of the

materials. The aforementioned phenomena that carboxylate-based electrodes show lower electrochemical potential (*vs*. Na/Na^+) than those of keto-carbonyl based materials further solidified our conclusion, because the $C\text{-}O^-$ group in the carboxylate is an electron-rich group. Therefore, higher electrochemical potential can be expected by utilizing more keto-carbonyl groups, which is apt to form suitable cathode materials and thereby makes the formation of higher voltage battery possible.

2.2 Determination of electrochemical window

The second aspect needed to take into concern for designing an electrode material in SIBs is the solubilities of the electrode material and its corresponding charged/discharged states in the electrolyte. There is no doubt that any slight dissolution of the material or its corresponding charged/discharged states will lead to significant performance degradation. In order to eliminate or decrease the dissolving of the electrode material as well as its corresponding charged/discharged states in the electrolyte, three possible methods could be adopted: 1) using polymeric materials; 2) the materials has the orthogonal intermiscibility with the electrolyte; 3) mixing with more conductive materials (or binder) or coating with Na^+-conductive materials (e.g. Al_2O_3 by atomic layer deposition). In a traditional organic electrolyte, the small molecular ionic compounds with orthogonal intermiscibility to the electrolyte is preferable to eliminate (rather than reduce) the dissolving, because the polymers are usually kind of soluble and need difficult, costly synthesis and purification and the third method is always ineffective for long time storage. Hence, we choose one material containing six keto-carbonyl groups ($(CO)_6$, **O1** in Figure 1) as a model here to demonstrate the important factors for fast-charge and -discharge sodium-ion batteries. It is clear that this charged state **O1** is inappropriate for the sodium-ion batteries because its solubility in the organic solvents.[17] Therefore, here, we utilize the material **DSR** (Figure 1, Table S1) and applied it in the sodium-ion batteries, offering a theoretical specific capacity of 501 mAh g^{-1}. In order to keep the material and corresponding charged/discharged states insoluble in the organic electrolyte, at least one of

the ionic bonds should be retained during the reduction/oxidization process. In another word, the electrode material **DSR** can only be reduced into its discharged state (**R1** in Figure 1) by accepting four electrons. Through these analyses, the range of the electrochemical window could be determined: the redox reaction should be shuttled between discharged state **R1** and charged state **DSR** (rather than charged state **O1**, Figure S1).

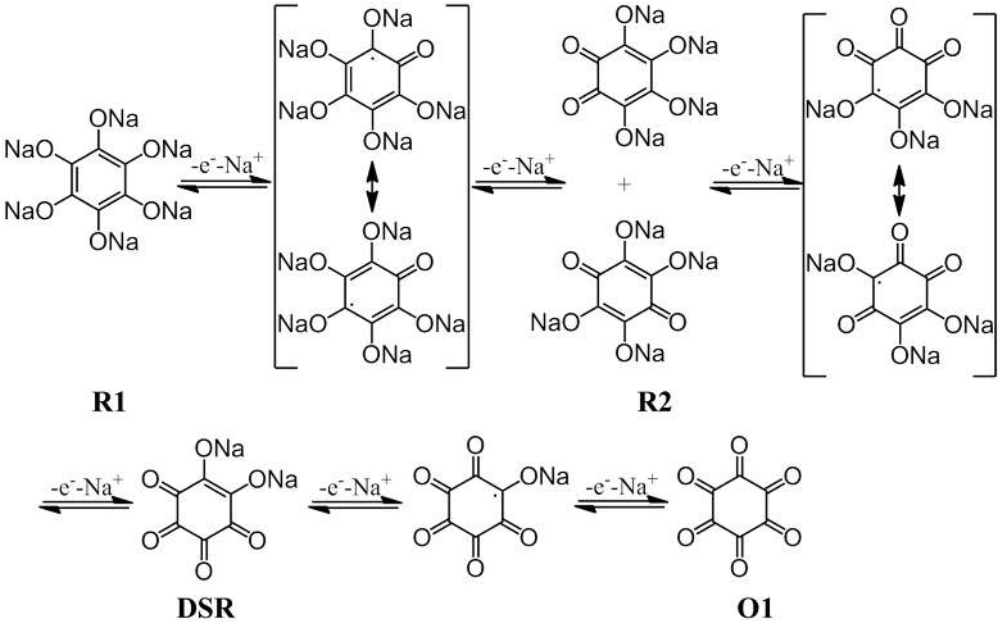

Figure 1. Schematic diagram of **DSR** and its discharged states (**R1** and **R2**) and potential charged state (**O1**), which involves six-electron transfer from **R1** to **O1**.

2.3 Ionic diffusion

The lithium salt of rhodizonate (**DLR**) was first[18, 19, 33-35] synthesized through low-cost and environmental friendly processes and applied as cathodes for LIBs. It has been found that the double bonds between carbon and oxygen (C=O) in the material **DLR** serves the redox centers for Li storage. Above, we already discussed the necessity and methodology of selecting the suitable electrochemical window which is determined by the solubility of the materials and related to four-electron redox reactions. Different from **DLR** which shows two pairs of redox peaks in Li-ion cells,[33] the typical CV curves of **DSR** exhibits four pairs of redox peaks with electrochemical potential located at ca. 1.80, 2.08, 2.32, 2.54 V respectively from the second cycles (Figure 2a). Although only one peak appeared in the first discharge

cycle (the reason will be discussed later), the CV curves became very stable afterwards. As shown in Figure 2a and 2b, all the four pairs of redox peaks (1, 2, 3 and 4) have almost identical anodic and cathodic currents with current ratio close to 1. The potential differences between the reduction and oxidization peaks of 1, 2 and 3 are around 0.03~0.05 V. The only exception is the current of cathodic peak 3 (C3) which increases a bit more than that of the anodic peak 3 (A3) with the scan rate increasing. Concurrently, the cathodic peak 4 (C4) shows negative shift to C3, leading to a lower peak potential of cathodic peak 4 (C4) and larger potential difference of redox peaks 4.

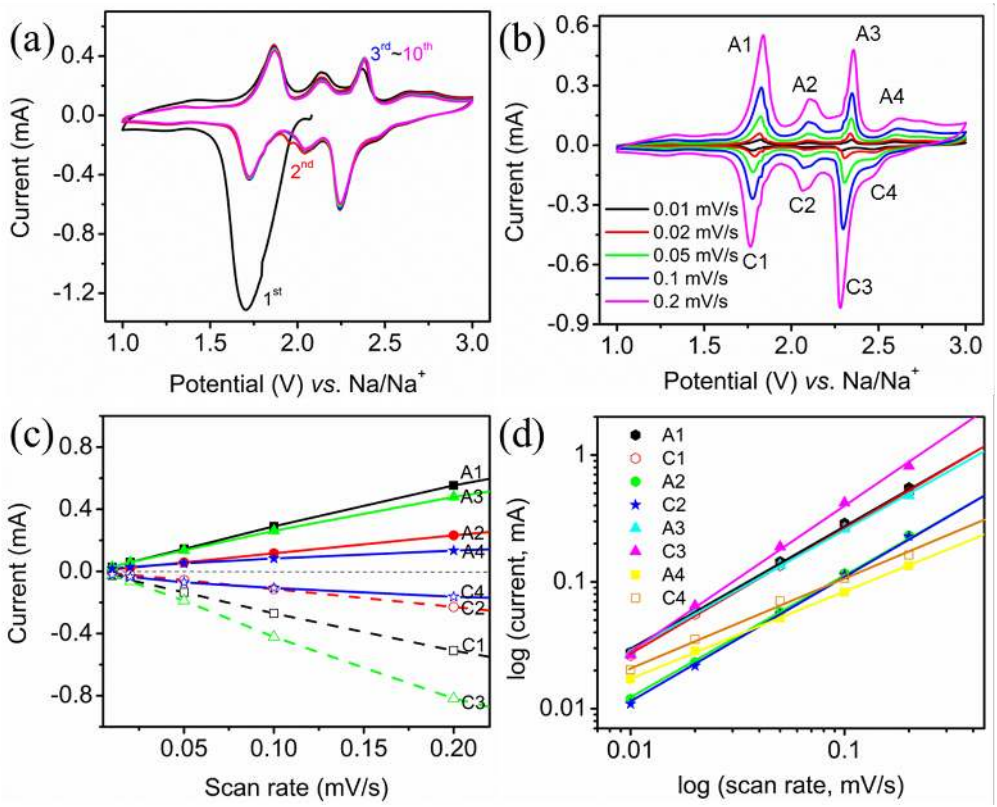

Figure 2. CV curves of **DSR** electrodes at a) a scan rate of 0.5 mV s^{-1} and b) different scan rates. More than three CV curves were measured for every scan rate, among which no obvious variation was observed. c) The linear relationship between the peak current and the scan rate. d) The log relationship of the peak current and the scan rate, of which the slope *b* can be used for determining the storage mechanism.

According to the Nernst equation, the peak potential (E_p) is dependent on the concentrations of the reduced [Red] and oxidized [Ox] species:

$$E_p = E_p^0 - \frac{RT}{nF} ln \frac{[Red]}{[Ox]}$$

and the potential difference (ΔE_p) between the reduction and oxidization peak of one revisable redox peaks at 25 °C should be close to or lower than $\frac{0.059}{n}$ V:

$$\Delta E_p = \left| E_{pa} - E_{pc} \right| = \frac{2.3RT}{nF} = \frac{0.059}{n} \text{ V}$$

where E_p^0, E_{pa} and E_{pc} are the standard potential, anodic peak potential and cathodic peak potential respectively, R is the gas constant, T is the absolute temperature, F is the Faraday constant and n is the number of electron transfer during the redox reaction.[36] Considering that the temperature during the scanning is lower than 25 °C (around 20 °C), it is reasonable to give the conclusion that the four pairs of redox processes are revisable or quasi-revisable and every pair redox peaks represents one electron reduction/oxidization (also see below). This is coincident with the schematic diagram of the electrochemical process as described in Figure 1. When the electrode material was reduced from **DSR** to compound **R1**, it is clear that the discharged states after accepted one (or three) electrons are not as stable as the discharged states after accepted two (or four) electrons. This probably can explain why the redox peaks 2 and 4 are smaller than 1 and 3. Simultaneously, this is also the probable reason that the potential of peak 4 during cathodic scan shifts to lower electrochemical potential (close to peak 3), leading to a higher potential difference of redox peak 4 and a higher reduction current of peak 3.

From Figure 2a, it is clear that the current is very stable after the second cycle. Such a stable and revisable electrochemical reaction makes it possible to acquire an in-depth understanding of the system by varying the scan rate. With the increase of the scan rate, the peak shapes keep almost invariable, although the currents increase consequently and potential

differences between the reduction and oxidization peaks are also increasing slightly. From Figure 2b, the cathodic and anodic peaks are almost symmetrical with each other for every redox peaks at any scan rates. Figure 2c and 2d present a more visual image that the cathodic and anodic peak currents are virtually identical, especially for the 1, 2 and 4 redox peaks. These suggest that the redox reactions keep quasi-reversible even at a higher scan rate. Most importantly, the peak currents increase proportionally to the scan rate rather than the square root of the scan rate (Figure 2c), which is different with **DLR** in lithium-ion batteries.[33] This result is very interesting because the proportion relationship between the peak current and the scan rate suggests that the sodium cell is not diffusion dominated but controlled by a capacitive effect. According to the equations:[37]

$$i = av^b$$

$$logi = b \times logv + loga$$

where i is the current density, v is the scan rate, and a and b are the adjustable parameters, when the slope b is close to 1, the system is mainly controlled by capacitance effect and when it approaches 0.5, the process is dominated by the diffusion of sodium ions. Figure 2d presents the log relationship of the current and the scan rate, which shows that all the slope b of the four-pairs peaks are close to 1 (as summarized in Table S2) and hence the **DSR** system is mainly controlled by a capacitive process. The attractive point behind this phenomenon is that the size of the sodium ions is larger than that of lithium ions; however, **DSR** system is more controlled by capacitive process rather than diffusion (the reason will be discussed below). The most important advantage of batteries to supercapacitors is their high energy densities and power densities. However, batteries always suffered a big problem, i.e. the slow charge and discharge efficiency, which is due to the difficulty of intercalation of lithium/sodium ions into the crystal lattice. This problem is particularly conspicuous for sodium ion batteries, leading to worse performances of SIBs than those of LIBs for the same materials, because sodium ions are much larger than lithium ions. Therefore, this capacitive

effect of the battery system is very meaningful, which can be expected to provide high performance for fast-charge and -discharge batteries.

2.4 Manipulation of binder

To investigate the capacitive effect on the battery performance, the electrochemical performance of **DSR** was studied by using a half-cell with sodium metal as the anode. The **DSR** electrodes were prepared by mixing **DSR** with carbon black (super-P) as conductive material and CMC as binder (weight ratio: 70:20:10) in water. Figure 3a shows the charge-discharge profiles of **DSR** electrodes between 3.0 and 1.0 V at a rate of 50 mA g^{-1}. The first discharge shows two plateaus located at ca. 2.0 and 1.8 V (the reason will be discussed later) and delivers a capacity of 264.7 mAh g^{-1}. However, the charge and discharge profiles afterwards show an average electrochemical potential of 2.1 V with four clear plateaus located at ca. 2.5, 2.3, 2.1 and 1.8 V respectively. These four plateaus agree well with the CV curves (2.54, 2.32, 2.08, 1.80V in Figure 2a-b), corresponding to the reversible oxidization/reduction of the four carbonyl groups with extraction/insertion of four Na cations. Similar to the CV curves, the plateaus around 2.5 and 2.1 V contributed much less capacities than the other two plateaus (2.3 and 1.8 V), probably due to the lower stabilities of the two discharged/charged states. One important point worthy noting is that the four plateaus in the charge profiles are almost symmetrical with the ones in the discharge profiles, suggesting the highly reversible properties of **DSR** in this electrochemical window. After the 2nd discharge, the capacity becomes stable with a capacity of about 173.5 mAh g^{-1}, giving a high Coulombic efficiency (CE) up to 94%. This capacity is among the highest capacities for organic cathodes (Table S3)[16, 17, 22-25]. From the 5th cycle, the Coulombic efficiency becomes higher than 98% (Figure 3b), giving a capacity as high as 168.9 mAh g^{-1} and keeping at 147.5 mAh g^{-1} after 100 cycles with a capacity retention higher than 80%. Although the capacity is comparatively lower than the theoretical specific capacity (such phenomena also can be found in other reports, as shown in Table S3. We are still working on this issue and the probable reason will

be discussed in the following), it is quite stable with high capacity retention. These phenomena were different with **DLR**-based LIBs[18, 19, 33, 34], which shows a very high initial capacity (close to the theoretical specific capacity) with significant degradation to similar level of revisable capacity (<200 mAh g^{-1} after 30 cycles). The capacity retention is much better than the **DSR** electrodes by using PVDF as binder[17] even with a lower electrochemical window (1.5~2.8 V). For the PVDF-based cells, a slight increase of the electrochemical window (1.5~2.9 V) will lead to a much lower capacity retention (64%, after 40 cycles) and the same electrochemical window with ours (1.0~3.0 V) results in a dramatically decrease of capacity retention to 36% (after 40 cycles). The degradation[17, 38] was ascribed to the dissolution of the electrode materials in the electrolyte and the damage of the electrode structure. However, our CMC-based **DSR** electrodes showed much higher capacity retention in sodium-ion batteries as mentioned above.

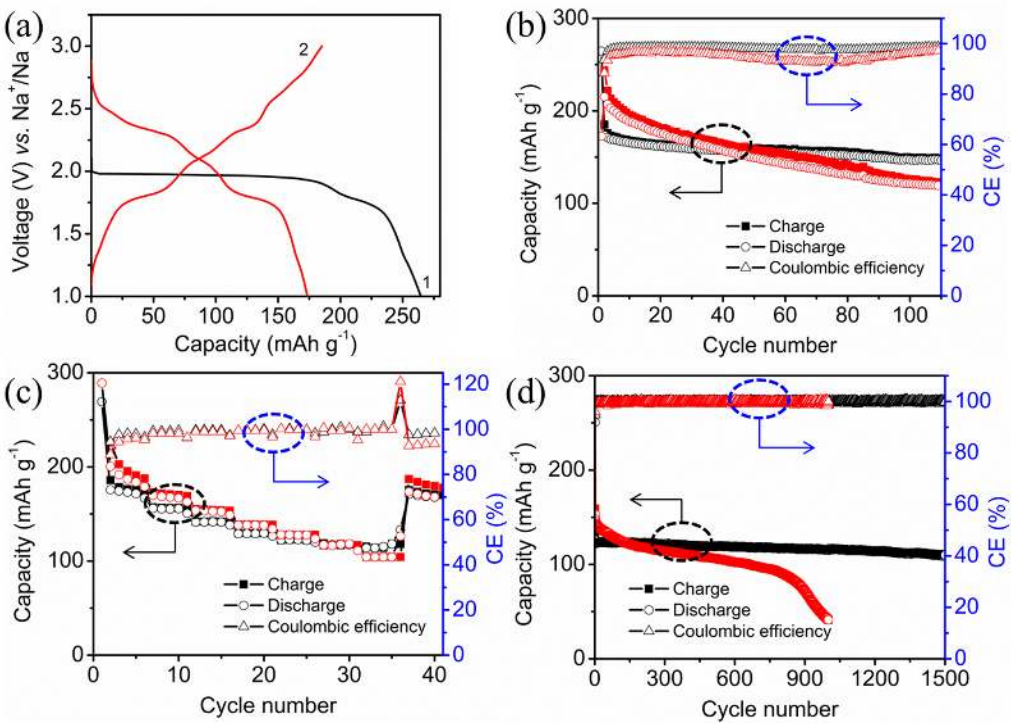

Figure 3. Electrochemical performances of **DSR**: a) voltage profiles of **DSR** electrodes by using CMC as the binder (only 1st and 2nd cycles are selected as representatives) at a rate of 50 mA g^{-1}. b) Cyclability at a rate of 50 mA g^{-1}, c) rate cyclability (left to right: from 50, 100,

200, 500, 1000, 2000, 5000 to 50 mA g^{-1}), and d) long-term cyclability at a rate of 1000 mA g^{-1} of **DSR** electrodes by using CMC and PVDF as the binder. b-d), black: CMC binder, red: PVDF binder.

In order to give a clear comparison, a control experiment was conducted by using PVDF in place of CMC as the binder and other conditions were kept as before. Figure 3b-d shows the comparison of **DSR** electrodes by using CMC and PVDF as binder respectively. The **DSR** electrodes using PVDF binder delivers a higher capacity of the 2nd discharge (215.2 mAh g^{-1}) at a rate of 50 mA g^{-1}. However, the capacity starts to decrease apparently from the second cycle and to 121.4 mAh g^{-1} after 100 cycles with a capacity retention as low as 56% (Figure 3b). Similar phenomena can also be observed during the fast-charge and -discharge processes. The electrodes with PVDF binder show higher capacity in the primary cycles than those with CMC binder. However, under fast-charge and -discharge processes, higher capacity was obtained in the electrodes with CMC binder. Remarkably, the capacity cycled at a rate of 5000 mA g^{-1} is still as high as 115 mAh g^{-1} for CMC-based electrodes and can be fully recovered afterwards. In this case, only 1 minute is needed for a full charge (Figure 3c and S2). Likewise, the long-term cyclabilities of **DSR** electrodes also exhibit similar phenomena (Figure 3d). The PVDF binder-based batteries display a higher capacity in the first 100 cycles at a rate of 1000 mA g^{-1}, but the capacity kept decreasing gradually afterwards and abrupt degradation were observed after 700 cycles. The capacity decreases from 153 mAh g^{-1} for the 2nd cycle to 44 mAh g^{-1} after 1000 cycles with retention as low as 29%. However, after 1000 cycles, the electrodes using CMC as the binder shows capacity still as high as 116 mAh g^{-1} with capacity retention up to 93%. Figure 3d shows the cyclability of a typical electrode with CMC as the binder cycled at a rate of 1000 mA g^{-1}. In this case, only 5 minutes are required for charging the batteries. It can be observed that even after 1500 cycles, the capacity is still as high as 110 mAh g^{-1}. Such a long-term cyclability with high capacity is remarkable for cathodes of fast-charge and -discharge sodium-ion batteries, which can guarantee a use more

than three years if charged once per day. These results suggest that our design strategy, i.e. the orthogonal intermiscibility, is undeniably helpful for improving the cyclability of the electrodes. What's more, our results also show that the capacity decay of the PVDF-based cells is probably due to the PVDF binder rather than the dissolution or structural damage of the electrodes. Further proofs of the degradation of the PVDF binder also could be found in literature[12] and the analyses below.

2.5 Charge transport

The effect of the conductive additive was also studied. The absence of carbon black (weight ratio of **DSR** and CMC: 90:10) failed to deliver storage of Na ions at a rate of 50 mA g^{-1}, which is probably due to the low charge transport. However, after adding carbon black, the performance is not evidently dependent on its content in the range from 10 to 30%. Higher carbon content was not examined because of the practical application concerns. There is no obvious difference between the samples by using different contents of the carbon black (10%, 20 % and 30%) for capacity, rate capacity and long-term cyclability (Figure S3-S5). All of them deliver a revisable capacity about 150 mAh g^{-1} even after 100 cycles at a rate of 50 mA g^{-1}. Remarkable long-term cyclabilities with low degradation after 1500 cycles were obtained for all of them under fast-charge and -discharge. These results suggest that all the capacity of the electrodes was contributed from the material itself and indicate that the charge transport from the electrode material to the current collector is not dominated in the charge/discharge process. The low resistance can be confirmed by the EIS studies. The EIS measurements were carried out in the frequency range from 1 MHz to 5 mHz for investigating the Na-ions diffusion from the electrolyte into the electrodes and the charge transfer from the electrodes to the current collector. The CMC-based electrodes show much lower resistance than PVDF-based electrodes (Figure S6). According to the morphology of the **DSR** electrodes (see below), the failure of the electrodes without the presence of conductive additive is probably due to the poor contact between the **DSR** crystals and the current collector, leading to a low charge

transport and high resistance between them. On the other hand, with the assistance of carbon black, the **DSR** materials can form low resistance and good charge transfer with the current collector, which probably is one of the reasons that the **DSR** electrodes show high capacity and high cyclability.

2.6 Elimination of water effect

It has been found that one **DLR** molecule (which was applied in LIBs) can combine two water molecules, forming a hydrate.[18, 19, 33] And this hydrate will decompose around 150~180 °C, by losing two water molecules, corresponding to a 16.5% weight loss. Therefore, the investigation of the potential formation of **DSR** hydrate is very important to the **DSR**-based SIBs, because water was utilized as the solvent during the fabrication process. However, different from **DLR**, there is no evidence that **DSR** also formed a hydrate. This conclusion can be approved by the TGA measurements. Two kinds of samples were utilized for TGA measurement: 1) the purchased samples without any treatment and 2) the samples were first dissolved in water and then dried at 110 °C in vacuum, according to the same process used for the preparation of the electrodes. There is no obvious difference between the two samples and the weight loss is negligible when the temperature is lower than 320 °C (<2 %) as shown in Figure 4, which means that a hydrate (the weight loss should be around 14.4%) is unlikely formed in our conditions. More importantly, the electrodes (with CMC as the binder) annealed at 185 °C in vacuum were also examined in SIBs for further verifying the absence of the hydrate in the electrode films. No obvious variation was observed between the electrodes with or without annealing.

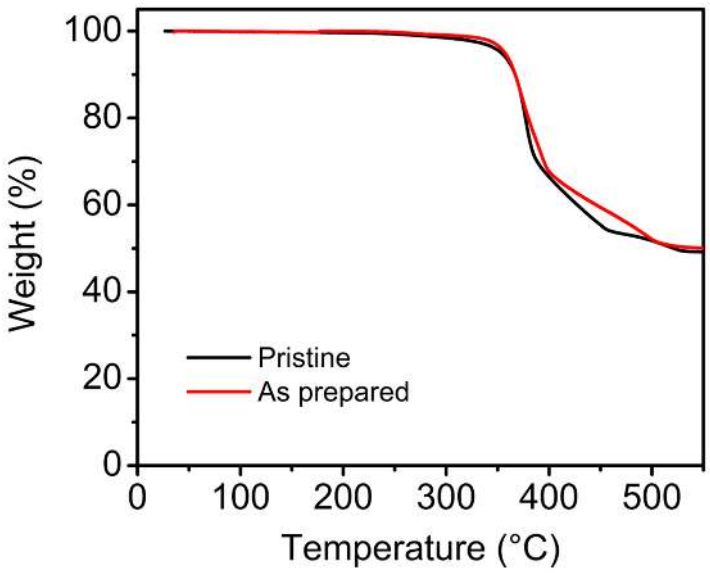

Figure 4. TGA curves of **DSR**. Black: the pristine **DSR** powder as purchased; red: **DSR** powder prepared according to the similar procedure of electrode fabrication.

2.7 Mechanism studies

In order to obtain a further insight of the **DSR** batteries to reveal the mechanism and the reason why it can provide high capacity and long-term cyclability, the ex-situ measurements of its SEM images, EDS spectra, XRD patterns and XPS spectra during the cycling are studied. Figure 5a-b shows the SEM images of **DSR** electrodes by using CMC as the binder as prepared and after cycling. It is clear that microcrystals with regular shape are formed by using water as the solvent (Figure 5a). The process is like a recrystallization, which forms morphology agreeing well with the theoretical simulated morphology by using Bravais−Friedel−Donnay−Harker (BFDH) rules (inset of Figure 5a).[39-41] However, the morphology changed significantly after it was discharged to 1.5 V (Figure 5b). Cracks appeared and a layer-by-layer morphology was formed. This is probably the reason that only one peak (Figure 2a) and two plateaus (Figure 3a) appeared in the first discharge cycle. The morphological deformation can be ascribed to the insertion of the large Na cations. Fortunately, the flexible nature and the strong intermolecular interactions guarantee the electrode structure from devastating. The formation of layer-by-layer morphology probably is

the reason that capacitive effect was observed in the **DSR** electrodes. This phenomenon is very interesting because it shows that the structural or morphology change is not equal to the performance degradation and the *in situ* formed flake morphology can lead to capacitive effect which is promising for fast-charge and -discharge batteries. Such capacitive effect or improvement of the diffusion was also reported by intentionally decreasing the particle size of the electrodes.[42, 43] On the other hand, the PVDF-based electrodes also showed similar morphology and morphology deformation (Figure S7), which indicates that the high performance from CMC binder is not due to the particle size, morphology or mixing homogeneity. Figure 5c and 5d show the EDS spectra and XRD patterns of the electrodes after discharge and charge processes. The EDS spectra (PVDF as binder) confirmed the storage mechanism is the redox reaction of the four carbonyl groups as discussed above. However, the XRD patterns show that the electrodes possess a different crystal phase after discharge to **R1**, which will recover to the initial state after recharge (Figure 5d), which is similar to the shuttled phase transition phenomenon as observed in **DLR**-based LIBs[33]. The difference is that the shuttled phase transition in **DLR**-based LIBs is a gradual change[33]; while the structure changes once the battery is charged (from **R1** to **DSR**) or discharged (from **DSR** to **R1**) (Figure S8). The reason probably can be ascribed to the larger size of sodium ions. Once the sodium ions are inserted into/extracted from the **DSR** materials, the crystal structure changed into another one. The difficulty of the insertion/extraction of the sodium ions is probably the reason that **DSR**-based SIBs show smaller capacity than the theoretical capacity. However, when the insertion/extraction of the sodium ions occurs, the fast adaptation of the crystal structure may benefit the fast-charge and -discharge performance.

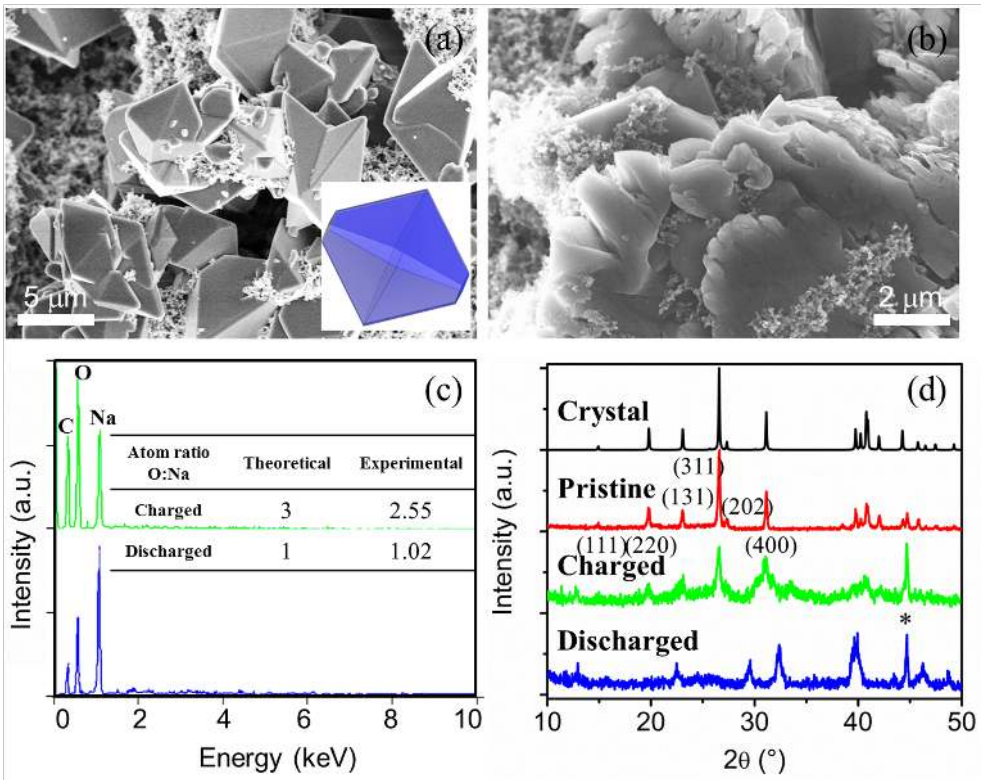

Figure 5. SEM images of **DSR** electrodes a) as prepared, inset of a): the simulated morphology of **DSR**; b) after discharged to 1.5 V at a rate of 50 mA g^{-1}. c) EDS spectra (top: charged state **DSR**, bottom: discharged state **R1**) and d) XRD patterns of charged (**DSR**) and discharged (**R1**) states (The peak marked by the star comes from the Al foil). Inset of c): the theoretical and experimental atom ratio of oxygen and sodium in the electrodes after charged and discharged.

Ex-situ measurements of XPS spectra were also conducted for monitoring the composition change during the charge/discharge process. Four states are measured, including the pristine state without cycling, the discharged state **R2** (discharged to 2.2 V, accepting two electrons and two sodium ions and forming a stable material **R2**), the discharged state **R1** (discharged to 1.5 V, accepting four electrons and four sodium ions and forming a stable material **R1**) and the charged state **DSR**. In order to reduce the experimental error, the charged state was selected in the same discharge cycle (discharged to 2.6 V, higher than the four plateaus), where the electrode material has not been reduced (see the voltage profile in Figure 3a) and hence equal to the charged state (**DSR**). It should be noted that because the elements C, O and

Na are in our concern, PVDF is used as the binder for eliminating the contamination from the CMC, which contains all these three elements. From the full range XPS spectra (Figure 6a), it is clear that from the discharged states **R1**, **R2** to the charged states **DSR**, the relative contents of carbon and oxygen are increasing compared with the content of sodium. This is coincident with the storage/extraction mechanism, as shown in Figure 1. The atom ratio between carbon/oxygen and sodium doesn't increase to the initial ratio as in the pristine samples, probably due to the degradation of the electrodes and the residual electrolyte (e.g. residual Cl_{2p} in Figure 6a) on the measured samples. The degradation of the electrodes and the decomposition of the PVDF can be clearly observed in the C_{1s} spectra (Figure 6b). There is only one peak around 291.2 eV in the pristine samples, corresponding to F-C-F groups. However, one new peak at 289.2 eV may appear which can be identified to H-C-F groups, or the peak may shift to around 290.0 eV probably belonging to CF_x (x=1~2). This can also be manifested by the relative decreasing content of the F to Na during the discharge process, as shown in Figure 6a. Although it has been proved that PVDF is very stable and is widely adopted as the binder in LIBs and SIBs, the results here show that PVDF will decompose in our conditions and the decomposition of PVDF is the reason for the degradation of PVDF-based electrodes rather than the dissolution of the materials or the morphology change. According to the storage mechanism as shown in Figure 1, the decomposition of PVDF in this situation probably can be ascribed to the possible nucleophilic substitution between the anion of **DSR** and the PVDF fluoride with the leaving of F anion[44]. Such nucleophilic substitution unlikely occurred in CMC-based electrodes due to the more difficulty of leaving for –OR group than –F group especially when **DSR** anions act as the nucleophile. Therefore, CMC binder should be stable in the same conditions, which is one of the reasons that long-term cycling stability can be achieved (also see Figure S6). On the other hand, from **R1**, **R2** to **DSR**, the electrode lost four electrons and four sodium cations, accompanying the increase of C=O and the decrease of C-O groups. This can be verified from the relative increased

intensity of C=O (287.1 eV) to C-O (285.9 eV) groups in the C_{1s} spectra (Figure 6b) and C=O (532.4 eV) to C-O (531.9 eV) in the O_{1s} spectra (Figure 6c). The Na_{1s} spectra can further confirm the formation of C-ONa (Figure 6d), corresponding to the peak around 1071.6 eV.

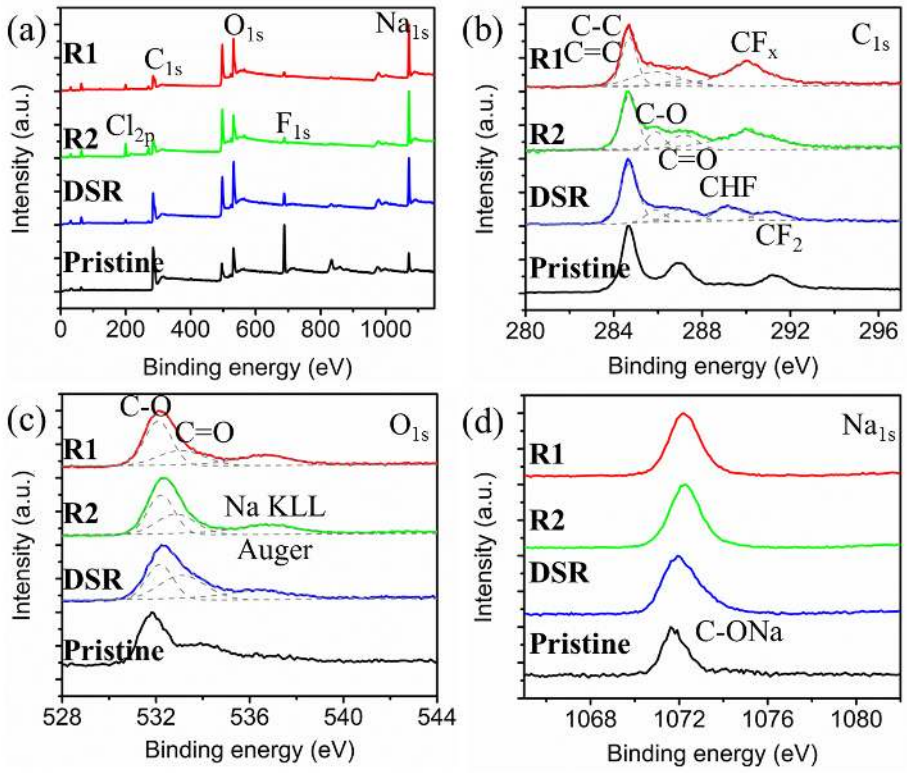

Figure 6. XPS spectra of **DSR** electrodes by using PVDF as the binder, from bottom to top: pristine sample without cycling (pristine), discharge to 2.6 V (**DSR**), 2.2 V (**R2**) and 1.5 V (**R1**) respectively: a) full range, b) C_{1s}, c) O_{1s} (the O_{1s} peak in the pristine sample is closer to C-O groups which can be contributed to the overlapping from Al_2O_3 (531.1 eV). This can be confirmed from the C_{1s} spectra, in which a clear peak appears around 286.9 eV corresponding to the C on native Al_2O_3 substrate. The peak around 536.8 eV probably can be ascribed to the sodium Auger peak) and d) Na_{1s}.

3. Conclusion

In conclusion, we have investigated the important factors for high performance fast-charge and -discharge batteries with high capacity and long-term cycleability by using **DSR** as a model. The molecular design for achieving high performance batteries and the importance and

strategy for eliminating the dissolving of the materials and improving the cyclability are discussed. By manipulating these important factors, the electrodes delivered a capacity of 173.5 mAh g^{-1} at a rate of 50 mA g^{-1}. Remarkably, a revisable capacity of 110 mAh g^{-1} was obtained even after charged/discharged 1500 cycles at a rate of 1000 mA g^{-1} with retention as high as 90%, which only needs 5 minutes for charging the batteries. This capacity is extraordinary for both organic LIBs and SIBs. Such a long-term cyclability with high capacity is outstanding for organic cathodes of fast-charge and -discharge sodium-ion batteries. The capacity cycled at 5000 mA g^{-1} is still as high as 115 mAh g^{-1} and can be fully recovered afterwards. We have found that controlling the solubility through molecular design and determination of the electrochemical window is essential to eliminating the dissolving of the electrode materials and thereby improving the cyclability. The XPS studies proved that PVDF will decompose during the charge/discharge process and its decomposition is the reason for the degradation of PVDF-based electrodes, indicating that suitable selection of binder is indispensable for achieving high cyclability. Decent charge transport and ionic diffusion are beneficial to the fast-charge and -discharge batteries, and flake morphology facilitates the ionic diffusion and thereby can lead to a capacitive effect that is favorable to fast-charge and -discharge. We believe that these studies can provoke stimulating interests of organic materials for high performance SIBs and pave a way to achieve practical application of SIBs in foreseeable large-scale flexible and wearable electronics.

4. Experimental Section

Characterization: The scanning electron microscopy (SEM) images and energy dispersive spectroscopy (EDS) spectra were obtained by using a Hitachi S4800 instrument applying voltages of 5 kV and 10 kV respectively. Thermogravimetric analysis (TGA) was recorded on a DTG-60 equipment (Shimadzu) under nitrogen atmosphere with a temperature gradient of 10 °C/min. The X-ray diffraction (XRD) measurements were measured on a Bruker-axs Discover D8 employing Cu Kα (1.54056 Å) radiation equipment. The cyclic voltammetry

(CV) and electrochemical impedance spectra (EIS) measurements were carried on a BioLogic VSP potentiostat. The CV spectra were scanned in the potential range from 1 to 3 V at different scan rates. The X-ray photoelectron spectroscopy (XPS) spectra were measured on a KRATOS Axis Ultra DLD spectrometer with a monochromatized Al Kα X-ray source (1486.6 eV) and an analyser pass energy of 20 eV at take-off angles of 90° under a pressure about 3×10^{-9} Torr. All samples were energy calibrated using the C_{1s} line at 284.7 eV. The ex-situ measurements are accomplished by immediately disassembling the batteries after charge/discharge and washing by propylene carbonate (PC) in N_2-filled glove box.

Electrochemical measurement: The sodium carboxymethyl cellulose (CMC)-based electrodes were fabricated by mixing **DSR** with carbon black (Super P) and CMC at different carbon contents (weight ratio: (90-x):x:10, x=0, 10, 20, 30), and then coated uniformly on an aluminum foil by using a doctor-blade with roughly 2 mg cm^{-2} mass loading. Water was used as the solvent. The poly(vinylidenedifluoride) (PVDF)-based samples for comparison, EDS and XPS spectra were prepared by mixing **DSR** with carbon black and PVDF in N-methyl-2-pyrrolidone (NMP). All the samples were dried at 110 °C under vacuum overnight. The electrochemical performance was evaluated by using R2032 coin cells with 1.0 M $NaClO_4$ in PC as the electrolyte solution. The batteries were assembled in a N_2-filled glove box with water and oxygen concentration lower than 0.1 ppm. Sodium metal was used as a counter electrode and glass fiber (Whatman, GF/B) was used as the separator. Galvanostatic experiments were performed at different current densities in a potential range of 1~3 V (vs. Na/Na^+) using a LANHE-CT2002A test system (Wuhan, China) under room temperature.

Supporting Information

Supporting Information is available from the Wiley Online Library or from the author.

Acknowledgements

The authors acknowledge the financial support from European Research Council (ThreeDsurface: 240144), BMBF (ZIK-3DNanoDevice: 03Z1MN11), BMBF (Meta-ZIK-BioLithoMorphie: 03Z1M511) and National Natural Science Foundation of China

(51203067). The authors also thank the help and discussion from Dr. Ye Zou, Mr. Xiaolong Fu and Ms. Moumou Li.

Received: ((will be filled in by the editorial staff))
Revised: ((will be filled in by the editorial staff))
Published online: ((will be filled in by the editorial staff))

[1] M. D. Slater, D. Kim, E. Lee, C. S. Johnson, *Adv. Funct. Mater.* **2013**, *23*, 947.

[2] N. Yabuuchi, K. Kubota, M. Dahbi, S. Komaba, *Chem. Rev.* **2014**, *114*, 11636.

[3] L. Liang, Y. Xu, C. Wang, L. Wen, Y. Fang, Y. Mi, M. Zhou, H. Zhao, Y. Lei, *Energy Environ. Sci.* **2015**, *8*, 2954.

[4] S.-W. Kim, D.-H. Seo, X. Ma, G. Ceder, K. Kang, *Adv. Energy Mater.* **2012**, *2*, 710.

[5] J. W. Wang, X. H. Liu, S. X. Mao, J. Y. Huang, *Nano Lett.* **2012**, *12*, 5897.

[6] Y. Xu, M. Zhou, X. Wang, C. Wang, L. Liang, F. Grote, M. Wu, Y. Mi, Y. Lei, *Angew. Chem. Int. Ed.* **2015**, *54*, 8768.

[7] Y.-N. Zhou, M. Sina, N. Pereira, X. Yu, G. G. Amatucci, X.-Q. Yang, F. Cosandey, K.-W. Nam, *Adv. Funct. Mater.* **2015**, *25*, 696.

[8] Z. Song, H. Zhou, *Energy Environ. Sci.* **2013**, *6*, 2280.

[9] Y. Liang, Z. Tao, J. Chen, *Adv. Energy Mater.* **2012**, *2*, 742.

[10] B. Häupler, A. Wild, U. S. Schubert, *Adv. Energy Mater.* **2015**, *5*, 1402034.

[11] M. Armand, S. Grugeon, H. Vezin, S. Laruelle, P. Ribiere, P. Poizot, J. M. Tarascon, *Nature Mater.* **2009**, *8*, 120.

[12] C. Wang, Y. Xu, Y. Fang, M. Zhou, L. Liang, S. Singh, H. Zhao, A. Schober, Y. Lei, *J. Am. Chem. Soc.* **2015**, *137*, 3124.

[13] A. Abouimrane, W. Weng, H. Eltayeb, Y. Cui, J. Niklas, O. Poluektov, K. Amine, *Energy Environ. Sci.* **2012**, *5*, 9632.

[14] Y. Park, D.-S. Shin, S. H. Woo, N. S. Choi, K. H. Shin, S. M. Oh, K. T. Lee, S. Y. Hong, *Adv. Mater.* **2012**, *24*, 3562.

[15] L. Zhao, J. Zhao, Y.-S. Hu, H. Li, Z. Zhou, M. Armand, L. Chen, *Adv. Energy Mater.* **2012**, *2*, 962.

[16] S. Wang, L. Wang, Z. Zhu, Z. Hu, Q. Zhao, J. Chen, *Angew. Chem. Int. Ed.* **2014**, *53*, 5892.

[17] K. Chihara, N. Chujo, A. Kitajou, S. Okada, *Electrochim. Acta* **2013**, *110*, 240.

[18] H. Chen, M. Armand, G. Demailly, F. Dolhem, P. Poizot, J.-M. Tarascon, *ChemSusChem* **2008**, *1*, 348.

[19] H. Chen, M. Armand, M. Courty, M. Jiang, C. P. Grey, F. Dolhem, J.-M. Tarascon, P. Poizot, *J. Am. Chem. Soc.* **2009**, *131*, 8984.

[20] H.-g. Wang, S. Yuan, D.-l. Ma, X.-l. Huang, F.-l. Meng, X.-b. Zhang, *Adv. Energy Mater.* **2014**, *4*, 1301651.

[21] A. Vlad, K. Arnould, B. Ernould, L. Sieuw, J. Rolland, J.-F. Gohy, *J. Mater. Chem. A* **2015**, *3*, 11189.

[22] Z. Song, Y. Qian, T. Zhang, M. Otani, H. Zhou, *Adv. Sci.* **2015**, DOI: 10.1002/advs.201500124.

[23] W. Luo, M. Allen, V. Raju, X. Ji, *Adv. Energy Mater.* **2014**, *4*, 1400554.

[24] W. Deng, X. Liang, X. Wu, J. Qian, Y. Cao, X. Ai, J. Feng, H. Yang, *Sci. Rep.* **2013**, *3*, 2671.

[25] K. Sakaushi, E. Hosono, G. Nickerl, T. Gemming, H. Zhou, S. Kaskel, J. Eckert, *Nature Commun.* **2013**, *4*, 1485.

[26] M. Yao, K. Kuratani, T. Kojima, N. Takeichi, H. Senoh, T. Kiyobayashi, *Sci. Rep.* **2014**, *4*, 3650.

[27] E. Castillo-Martínez, J. Carretero-González, M. Armand, *Angew. Chem. Int. Ed.* **2014**, *53*, 5341.

[28] W. Walker, S. Grugeon, O. Mentre, S. Laruelle, J.-M. Tarascon, F. Wudl, *J. Am. Chem. Soc.* **2010**, *132*, 6517.

[29] T. Nokami, T. Matsuo, Y. Inatomi, N. Hojo, T. Tsukagoshi, H. Yoshizawa, A. Shimizu, H. Kuramoto, K. Komae, H. Tsuyama, J.-i. Yoshida, *J. Am. Chem. Soc.* **2012**, *134*, 19694.

[30] Y. Liang, P. Zhang, S. Yang, Z. Tao, J. Chen, *Adv. Energy Mater.* **2013**, *3*, 600.

[31] C. Luo, R. Huang, R. Kevorkyants, M. Pavanello, H. He, C. Wang, *Nano Lett.* **2014**, *14*, 1596.

[32] M. Lopez-Herraiz, E. Castillo-Martinez, J. Carretero-Gonzalez, J. Carrasco, T. Rojo, M. Armand, *Energy Environ. Sci.* **2015**, *8*, 3233.

[33] H. Kim, D.-H. Seo, G. Yoon, W. A. Goddard, Y. S. Lee, W.-S. Yoon, K. Kang, *J. Phys. Chem. Lett.* **2014**, *5*, 3086.

[34] S. Gottis, A.-L. Barrès, F. Dolhem, P. Poizot, *ACS Appl. Mater. Interfaces* **2014**, *6*, 10870.

[35] N. Raveta, C. Michota, M. Armanda, *Mat. Res. Soc. Symp. Proc.* **1998**, *496*, 263.

[36] D. K. Gosser, *Cyclic Voltammetry*, VCH Publishers, Inc., New York **1994**.

[37] Z. Hu, L. Wang, K. Zhang, J. Wang, F. Cheng, Z. Tao, J. Chen, *Angew. Chem. Int. Ed.* **2014**, *53*, 12794.

[38] X. Xiang, K. Zhang, J. Chen, *Adv. Mater.* **2015**, *37*, 5343.

[39] C. Wang, H. Dong, W. Hu, Y. Liu, D. Zhu, *Chem. Rev.* **2012**, *112*, 2208.

[40] C. Wang, Y. Liu, Z. Ji, E. Wang, R. Li, H. Jiang, Q. Tang, H. Li, W. Hu, *Chem. Mater.* **2009**, *21*, 2840.

[41] J. D. H. Donnay, D. Harker, *Am. Mineral.* **1937**, *22*, 446.

[42] F. Wan, X.-L. Wu, J.-Z. Guo, J.-Y. Li, J.-P. Zhang, L. Niu, R.-S. Wang, *Nano Energy* **2015**, *13*, 450.

[43] C. Luo, Y. Zhu, Y. Xu, Y. Liu, T. Gao, J. Wang, C. Wang, *J. Power Sources* **2014**, *250*, 372.

[44] V. M. Vlasov, *J. Fluorine Chem.* **1993**, *61*, 193.